

SEGMENTATION OF IMAGES PAINTED ON PARAMETRIC MANIFOLDS

Alon Spira and Ron Kimmel

Department of Computer Science, Technion
Haifa, Israel
email: {salon,ron}@cs.technion.ac.il

ABSTRACT

Active contours are a widely spread tool for the important task of image segmentation. An active contour evolves in time on an image, till it stops on the boundaries of the objects in it. The forces governing this evolution consist of internal geometric forces and external forces originating from the image data.

We present the use of active contours for the segmentation of a more general type of images, i.e., images painted on parametric manifolds. Good representatives of this kind of images are face images, where the face manifold is a 2-dimensional manifold embedded in a Euclidean 3-dimensional space. Adding the manifold data can be most beneficial in various tasks including face recognition and enables also a better segmentation of face features such as eyes.

We show that taking into account the geometry of the manifold boosts the performance of active contours. The inclusion of the manifold's geometry is done by evolving the contour on the manifold, instead of on a flat planar image. To keep the contour on the manifold the geodesic components of the driving forces are used.

Appropriate numerical schemes enable the robust implementation of these active contours. Added efficiency is gained by evolving the active contours on the 2-dimensional cartesian parameterization plane and projecting the result back to the manifold.

1. INTRODUCTION

Active contours for image segmentation ('snakes') were introduced by Kass et. al. [13]. Geometric active contours formulated and implemented based on the level set method [20] were presented by Caselles et. al. [3] and Malladi et. al. [19]. The first incorporation of a geometric (re-parameterization invariant) functional minimization was done in the geodesic active contour model of Caselles et. al. [4] where the functional

$$\int_0^L f(c(s)) ds \quad (1)$$

using the edge sensitive weighting

$$f(|\nabla I|) = \frac{1}{1 + \frac{|\nabla I|^2}{\lambda^2}}, \quad (2)$$

of the image I is minimized by the Euler-Lagrange equations

$$C_t = (\kappa f - \langle \nabla f, N \rangle) N, \quad (3)$$

with κ the curvature of the contour C , s its arc length, L its length and N its normal. The first term on the right hand side of Equation (3) is the geodesic curvature flow. The second term is geodesic advection. The level set representation [20] of the equation is

$$\phi_t = f \cdot \operatorname{div} \left(\frac{\nabla \phi}{|\nabla \phi|} \right) |\nabla \phi| + \langle \nabla f, \nabla \phi \rangle. \quad (4)$$

Additional developments followed, including [18, 5, 6, 11, 16, 10].

Our objective is to extend the geodesic active contour model for images painted on manifolds. Incorporating the manifold's geometry into the active contour can improve the segmentation for images that originate from their manifolds, such as face images. Since the driving forces of the geodesic active contour are the curvature flow and advection, as evident from Equation (3), the extended version will necessitate an implementation of their geodesic counterparts.

There are two main approaches in the previous work done on the implementation of these geodesic flows. According to the first approach [8, 15, 17, 14] the geodesic curvature flow is implemented for function graphs by projecting the PDEs to \mathbb{R}^2 , performing the numerical calculations there and then mapping back the solutions to the manifold. A more general approach for the motion of curves on manifolds was developed by [7, 1]. Their approach is to implicitly represent both the manifold and the curve or data on it as level sets of functions in \mathbb{R}^N . The level set representing the manifold is static and the level set representing the curve or the data is moving according to the PDE. This approach has several drawbacks, see [21].

We solve the problems of the later approach by following in the footsteps of the first approach. We back project the flow from the manifold to the parameterization plane, solve on the plane and then map the result back to the manifold. The complexity of the calculations is not affected by the dimension of the space in which the manifold is embedded and the approach is suited for all manifolds, including self intersecting ones.

2. DEFINITIONS AND MOTIVATION

We consider a parameterization plane $U = \{u^1, u^2\} \in \mathbb{R}^2$. This plane is mapped by $X : \mathbb{R}^2 \rightarrow \mathbb{R}^N$ to the parametric manifold $X(U) = \{x^1(u^1, u^2), x^2(u^1, u^2), \dots, x^N(u^1, u^2)\} \in \mathbb{R}^N$. Any curve $C(s) \in X(U)$ has an origin $\tilde{C}(\tilde{s}) \in U$, i.e., each point $p \in C(s)$ is a mapping of a corresponding point $\tilde{p} \in \tilde{C}(\tilde{s})$ by $p = X(\tilde{p})$. s and \tilde{s} are the arc length parameterizations of the curves C and \tilde{C} respectively. The derivatives of X with respect to u^i are defined as $X_i \triangleq \frac{\partial X}{\partial u^i}$. See Figure 1.

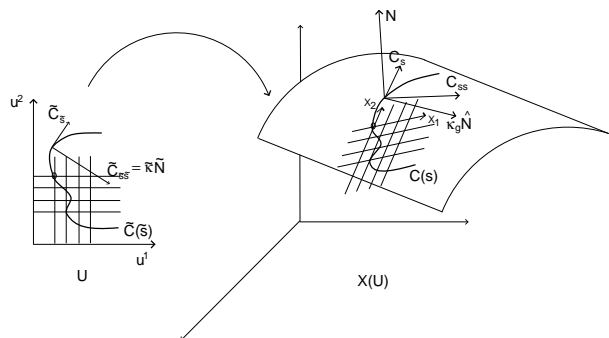


Figure 1: The curve $C(s)$ on the manifold $X(U)$ and its origin $\tilde{C}(\tilde{s})$ on the parameterization plane U .

The distance element on the manifold is

$$ds = \sqrt{g_{ij} du^i du^j}, \quad (5)$$

where we use Einstein's summation convention, the metric tensor of the manifold g_{ij} is calculated by

$$(g_{ij}) = \begin{pmatrix} g_{11} & g_{12} \\ g_{21} & g_{22} \end{pmatrix} = \begin{pmatrix} X_1 \cdot X_1 & X_1 \cdot X_2 \\ X_2 \cdot X_1 & X_2 \cdot X_2 \end{pmatrix}, \quad (6)$$

and $g = \det(g_{ij}) = g_{11}g_{22} - g_{12}^2$.

According to the above definitions, the derivative of $C(s)$ with respect to its arc length is C_s , which is the tangent to the curve C . Similarly, we have $\tilde{C}_{\tilde{s}}$, which is the tangent to $\tilde{C}(\tilde{s})$. We denote by N the normal to the plane tangent to the manifold $X(U)$ and in the direction of $X_1 \times X_2$. \hat{N} is the unit vector normal to the curve $C(s)$ lying in that plane. \tilde{N} represents the normal to $\tilde{C}_{\tilde{s}}$ in the plane U .

3. TRANSFORMING FLOWS ON MANIFOLDS TO FLOWS ON THE PARAMETERIZATION PLANE

Any geometric flow of the curve $C(s)$ of the form $C_t = F\hat{N}$, has a corresponding geometric flow on U of the form $\tilde{C}_t = \tilde{F}\tilde{N}$. If we can find \tilde{F} as a function of F and the mapping X , we can simplify the calculation of the flow on $X(U)$ by performing the flow on U and then mapping the result onto $X(U)$. To enable this, we represent vectors in the N -dimensional space according to the basis $\{X_1, X_2\}$. The other components of the vectors, which are perpendicular to X_1 and X_2 , do not affect the flow of the curve $C(s)$ on the manifold $X(U)$.

3.1 Geodesic Curvature Flow

We start with the geodesic curvature flow of $C(s)$

$$C_t = \kappa_g \hat{N} = C_{ss} - \langle C_{ss}, N \rangle N. \quad (7)$$

This is the flow of the curve $C(s)$ according to the component of its curvature, tangent to the manifold $X(U)$. Taking only this component of the curvature keeps the curve on the manifold.

The derivation of the geodesic curvature flow as a flow on the parameterization plane was introduced in [21]. Only the main steps are given here. First, C_s is represented according to the basis $\{X_1, X_2, N\}$

$$C_s = u_s^i X_i. \quad (8)$$

By differentiating this expression with respect to s we get

$$C_{ss} = u_{ss}^i X_i + u_s^i (\Gamma_{ij}^k X_k + b_{ij} N) u_s^j, \quad (9)$$

with Γ_{ij}^k being Christoffel's symbols and b_{ij} the coefficients of the second fundamental form [2]. $\kappa_g \hat{N}$ is the component of C_{ss} in the plane tangent to $X(U)$

$$\kappa_g \hat{N} = \left(u_{ss}^k + \Gamma_{ij}^k u_s^i u_s^j \right) X_k. \quad (10)$$

We use the chain rule to compute

$$C_t = X_k u_t^k \quad (11)$$

and after a few manipulations we get the flow on the parameterization plane

$$\tilde{C}_t = q_s C_{\tilde{s}} + q^2 \left(C_{\tilde{s}\tilde{s}} + \{ \Gamma_{ij}^k u_{\tilde{s}}^i u_{\tilde{s}}^j, \Gamma_{ij}^k u_{\tilde{s}}^i u_{\tilde{s}}^j \} \right), \quad (12)$$

with $q \triangleq \frac{\partial \tilde{s}}{\partial s}$. But the geometric flow depends only on the component of \tilde{C}_t in the direction of \tilde{N} , i.e.

$$\langle \tilde{C}_t, \tilde{N} \rangle = \frac{\tilde{\kappa} + \langle \{ \Gamma_{ij}^k u_{\tilde{s}}^i u_{\tilde{s}}^j, \Gamma_{ij}^k u_{\tilde{s}}^i u_{\tilde{s}}^j \}, \tilde{N} \rangle}{g_{ij} u_{\tilde{s}}^i u_{\tilde{s}}^j}, \quad (13)$$

where $\tilde{\kappa}$ is the curvature of \tilde{C} .

3.2 Geodesic Advection

The second flow is the geodesic advection of $C(s)$

$$C_t = V, \quad (14)$$

where V is an external vector field, i.e., V is independent of the curve $C(s)$.

The representation of V according to the basis $\{X_1, X_2\}$ is

$$V = b^i X_i. \quad (15)$$

The scalar products between V and the vectors X_i are

$$v_i \triangleq \langle V, X_i \rangle = b^j g_{ij}. \quad (16)$$

A few manipulations yield

$$b^1 = \frac{v_1 g_{22} - v_2 g_{12}}{g}, \quad b^2 = \frac{v_2 g_{11} - v_1 g_{12}}{g}. \quad (17)$$

The resulting equation for the flow is

$$\tilde{C}_t = \{v_1 g^{11} + v_2 g^{12}, v_2 g^{22} + v_1 g^{12}\}, \quad (18)$$

where g^{ij} are the components of the contravariant metric tensor, which is the inverse of the metric tensor. This flow is an advection on the parameterization plane.

4. LEVEL SET REPRESENTATION OF THE FLOWS

We next convert the flow equations we got in the previous section into level set equations [20]. This formulation enjoys many numerical advantages.

4.1 Geodesic Curvature Flow

For the geodesic curvature flow this means converting Equation (13) to a level set formulation. We assume that $\tilde{C}(\tilde{s}) = \{u^1(\tilde{s}), u^2(\tilde{s})\}$ is the zero set of $\phi(u^1, u^2)$. This means

$$\phi_t = \frac{\tilde{\kappa} + \langle \{ \Gamma_{ij}^k u_{\tilde{s}}^i u_{\tilde{s}}^j, \Gamma_{ij}^k u_{\tilde{s}}^i u_{\tilde{s}}^j \}, \tilde{N} \rangle}{g_{ij} u_{\tilde{s}}^i u_{\tilde{s}}^j} |\nabla \phi|. \quad (19)$$

To develop the expressions in the right hand side of Equation (19) as functions of ϕ , X , and their spatial derivatives we use the relation

$$\{-u_{\tilde{s}}^2, u_{\tilde{s}}^1\} = \tilde{N} = \frac{\nabla \phi}{|\nabla \phi|}, \quad (20)$$

and get

$$u_{\tilde{s}}^1 = \frac{\phi_2}{(\phi_1^2 + \phi_2^2)^{\frac{1}{2}}}, \quad u_{\tilde{s}}^2 = \frac{-\phi_1}{(\phi_1^2 + \phi_2^2)^{\frac{1}{2}}} \quad (21)$$

and

$$\tilde{\kappa} = \text{div} \left(\frac{\nabla \phi}{|\nabla \phi|} \right) = \frac{\phi_1^2 \phi_{22} - 2\phi_1 \phi_2 \phi_{12} + \phi_2^2 \phi_{11}}{(\phi_1^2 + \phi_2^2)^{\frac{3}{2}}}. \quad (22)$$

After some work we get

$$\phi_t = \frac{(-1)^{(i-j)} \phi_i \phi_j \phi_{|3-i||3-j|}}{g |\nabla_M \phi|^2} + \frac{(-1)^{(i-j)} \Gamma_{ij}^k \phi_{|3-i|} \phi_{|3-j|} \phi_k}{g |\nabla_M \phi|^2} \quad (23)$$

with Christoffel's symbols calculated by derivatives of the first fundamental form

$$\Gamma_{ij}^k = \frac{1}{2} g^{kl} (\partial_i g_{lj} + \partial_j g_{il} - \partial_l g_{ij}). \quad (24)$$

4.2 Geodesic Advection

The level set representation of the planar flow equation

$$\tilde{C}_t = \tilde{V} \quad (25)$$

is

$$\phi_t = \langle \tilde{V}, \nabla \phi \rangle. \quad (26)$$

Therefore, the level set representation of Equation (18) is

$$\phi_t = \left(v_1 g^{11} + v_2 g^{12} \right) \phi_1 + \left(v_2 g^{22} + v_1 g^{12} \right) \phi_2. \quad (27)$$

5. THE NUMERICAL SCHEMES

The implementation of the level set equations on the parameterization plane necessitates appropriate numerical schemes. These schemes are presented in this section.

5.1 Geodesic Curvature Flow

We start with a numerical scheme for Equation (23). The first term on the right hand side of this equation is diffusive and can be implemented with central differences. The second term is a non-convex hyperbolic term and needs a special numerical scheme.

We used a fifth order Weighted Essentially Non-Oscillatory (WENO) scheme with a global Lax-Friedrichs (LF) flux in space [12] and a third order Total Variation Diminishing Runge-Kutta (TVD-RK) scheme in time. Non-periodic boundary conditions were used.

A re-distancing of the level set function was activated every few iterations, as a regularizing process. The re-distancing was accomplished by the Sussman-Fatemi method [23]. This method uses the equation

$$\phi_t = \text{sign}(\phi_0) (1 - |\nabla \phi|) \quad (28)$$

to transform the level set function ϕ_0 into a distance map. Also this equation is implemented by a fifth order WENO-LF, third order TVD-RK numerical scheme. The zero set of ϕ_0 is maintained by applying a volume conserving condition of the form

$$\partial_t \int_{\Omega} H(\phi) = 0, \quad (29)$$

with H the Heaviside function and Ω a fixed domain. The condition is applied by using a gradient projection step.

5.2 Geodesic Advection

For a moving curve represented by the level set function ϕ , the value of ϕ does not change along the curve. If we apply this to the curve moving on the parameterization plane, we get

$$0 = \frac{d\phi}{dt} = \frac{\partial \phi}{\partial t} + \frac{\partial \phi}{\partial u^1} \underbrace{\frac{du^1}{dt}}_{v_{u^1}} + \frac{\partial \phi}{\partial u^2} \underbrace{\frac{du^2}{dt}}_{v_{u^2}}, \quad (30)$$

with v_{u^i} being the speed of the curve in the direction of the parameter u^i . Comparing Equation (30) with Equation (27) yields

$$v_{u^1} = v_1 g^{11} + v_2 g^{12} \quad (31)$$

and

$$v_{u^2} = v_2 g^{22} + v_1 g^{12}. \quad (32)$$

An appropriate upwind numerical scheme for the component in the u^i direction is

$$v_{u^i} \phi_{u^i} \approx \max(v_{u^i}, 0) D_{u^i}^- \phi + \min(v_{u^i}, 0) D_{u^i}^+ \phi, \quad (33)$$

with $D_{u^i}^-$ the backward difference in the u^i direction and $D_{u^i}^+$ the forward difference in the same direction.

6. GEODESIC ACTIVE CONTOURS ON MANIFOLDS

The geodesic extension of Equation (3) is

$$C_t = (\kappa_g f - \langle \nabla f, \hat{N} \rangle) \hat{N}, \quad (34)$$

with \hat{N} the projection of the normal to the contour on the plane tangent to manifold M . The weighting function f stays as in Equation (2). Replacing κ with κ_g in Equation (3) and using \hat{N} instead of N are necessary in order to keep the active contour on the manifold.

The geodesic curvature flow, which is the first term on the right hand side of Equation (34), is a curve shortening flow. Its role is to contract the curve. The weighting function f that multiplies it stops the contraction at the image edges. The geodesic advection, which is the second term on the right hand side of Equation (34), is not active where the amplitude of the image edge ($|\nabla I|$) is constant since there $\nabla f = 0$. It comes into action in the vicinity of the edge and pulls the active contour to the maximum of the edge.

This flow is implemented numerically by performing the calculations on the parameterization plane. For the second term on the right hand side of Equation (34) we can identify V from Equation (14) to be

$$V = \nabla f, \quad (35)$$

yielding

$$v_i \triangleq \langle V, X_i \rangle = \langle \left\{ \frac{\partial f}{\partial x^1}, \dots, \frac{\partial f}{\partial x^N} \right\}, \left\{ \frac{\partial x^1}{\partial u^i}, \dots, \frac{\partial x^N}{\partial u^i} \right\} \rangle = \frac{\partial f}{\partial u^i} \triangleq f_i. \quad (36)$$

Combining this with Equations (31,32) gives

$$v_{u^1} = g^{11} f_1 + g^{12} f_2 \quad (37)$$

and

$$v_{u^2} = g^{22} f_2 + g^{12} f_1. \quad (38)$$

Plugging this into Equation (27) and using Equation (23) for the first term on the right hand side of Equation (34) gives the following level set equation on the parameterization plane

$$\begin{aligned} \phi_t = & f \left[\frac{(-1)^{(i-j)} \phi_j \phi_{|3-j|} \phi_{|3-j|}}{g |\nabla_M \phi|^2} + \frac{(-1)^{(i-j)} \Gamma_{ij}^k \phi_{|3-j|} \phi_{|3-j|} \phi_k}{g |\nabla_M \phi|^2} \right] + \\ & \left(f_m g^{mm} + f_{(3-m)} g^{12} \right) \phi_m. \end{aligned} \quad (39)$$

This equation is solved using the numerical schemes described in the previous section.

7. SIMULATIONS AND RESULTS

Figure 2 shows the performance of the geodesic active contour model for an image painted on a Klein bottle. The image of a square is painted on the parameterization plane and projected to the manifold to create the image appearing on the Klein bottle in the figure. The original contour is a concentric circle on the parameterization plane. It contracts till it stops on the edges of the square, thus segmenting it from the image's background.

It can be seen from Figure 2 that the contour does not reach completely all the edges of the square. The reason is that the sections of the contour at these locations are geodesics ($\kappa_g = 0$ locally). This problem is sometimes solved by itself due to the force applied on the edge points of the problematic contour section. This can be seen on the handle of the Klein bottle in the second and third images of Figure 2.

The problem of the active contour stopping in a local minimum is a known phenomena of the geodesic active contour model. A popular remedy for this problem is adding a time dependent constant velocity term in the spirit of the "balloon force" introduced by Cohen [9].

In real life images the active contour may stop on false edges caused by noise. Image smoothing is used as a pre-process in these cases in order to get rid of the excess noise. A suitable method for smoothing images painted on manifolds is presented in [22].

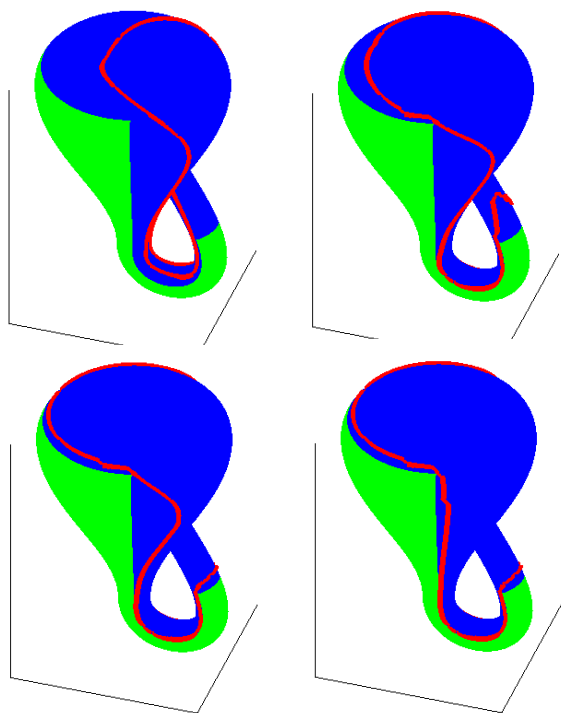


Figure 2: The performance of the geodesic active contour model for an image painted on a Klein bottle. The order of the images is from top to bottom and left to right.

8. CONCLUSIONS AND FUTURE WORK

We have introduced the segmentation of images painted on parametric manifolds by using a geodesic active contour model. The implementation of the model requires appropriate numerical schemes for the geodesic curvature flow and geodesic advection. We have shown that efficient and robust numerical schemes can be devised by projecting the flows from the manifold to its parameterization plane and performing the calculations there. The segmentation was demonstrated for synthetic manifolds.

This work is a proof of concept. We intend to use the approach presented here to extend more advanced active contour models to images painted on manifolds and to use them for real life applications, such as face image segmentation.

REFERENCES

- [1] M. Bertalmio, L. Cheng, S. Osher, and G. Sapiro. Variational problems and partial differential equations on implicit surfaces. *Journal of Computational Physics*, 174:759–780, October 2001.
- [2] M. D. Carmo. *Differential Geometry of Curves and Surfaces*. Prentice-Hall, New Jersey, USA, 1976.
- [3] V. Caselles, F. Catte, T. Coll, and F. Dibos. A geometric model for active contours. *Numerische Mathematik*, 66:1–31, 1993.
- [4] V. Caselles, R. Kimmel, and G. Sapiro. Geodesic active contours. *International Journal of Computer Vision*, 22(1):61–79, 1997.
- [5] V. Caselles, R. Kimmel, G. Sapiro, and C. Sbert. Minimal surfaces based object segmentation. *IEEE Trans. on Pattern Analysis Machine Intel.*, 19(4):394, 1997.
- [6] T. Chan and L. Vese. Active contours without edges. *IEEE Trans. on Image Processing*, 10(2):266–277, 2001.

- [7] L. Cheng, P. Burchard, B. Merriman, and S. Osher. Motion of curves constrained on surfaces using a level set approach. *Journal of Comp. Physics*, 175(2):604–644, 2002.
- [8] D. Chopp and J. Sethian. Flow under curvature: Singularity formation, minimal surfaces, and geodesics. *J. Exper. Math.*, 2(4):235–255, 1993.
- [9] L. Cohen. On active contour models and balloons. *CVGIP: Image Understanding*, 53(2):211–218, 1991.
- [10] B. Gilburd, M. Holtzman-Gazit, A. Spira, D. Goldsher, and R. Kimmel. Volumetric medical imaging environment. In *Proc. of Dicta 2003*, Sydney, Australia, December 2003.
- [11] R. Goldenberg, R. Kimmel, E. Rivlin, and M. Rudsky. Fast geodesic active contours. *IEEE Trans. on Image Processing*, 10(10):1467–1475, 2001.
- [12] G. Jiang and D. Peng. Weighted ENO schemes for hamilton-jacobi equations. *SIAM J. Sci. Comput.*, 21(6):2126–2143, 2000.
- [13] M. Kass, A. Witkin, and D. Terzopoulos. Snakes: Active contour models. *Int. J. Comput. Vis.*, 1:321–331, 1988.
- [14] R. Kimmel. Intrinsic scale space for images on surfaces: The geodesic curvature flow. *Graphical Models and Image Processing*, 59(5):365–372, 1997.
- [15] R. Kimmel, A. Amir, and A. Bruckstein. Finding shortest paths on surfaces using level sets propagation. *IEEE Trans. on PAMI*, 17(1):635–640, 1995.
- [16] R. Kimmel and A. Bruckstein. On regularized laplacian zero crossings and other optimal edge integrators. *Int. Journal of Computer Vision*, 53(3):225–243, 2003.
- [17] R. Kimmel and N. Kiryati. Finding shortest paths on surfaces by fast global approximation and precise local refinement. *Int. Journal of Pattern Recognition and Artificial Intelligence*, 10(6):643–656, 1996.
- [18] R. Malladi and J. Sethian. An $O(N \log(N))$ algorithm for shape modeling. *Proc. of National Academy of Sciences*, 93:9389–9392, Sep. 1996.
- [19] R. Malladi, J. Sethian, and B. Vemuri. Shape modeling with front propagation: a level set approach. *IEEE T. Patt. Anal. Mach. Intell.*, 17(2):158–175, 1995.
- [20] S. Osher and J. Sethian. Fronts propagation with curvature dependent speed: Algorithms based on hamilton-jacobi formulations. *J. Comput. Phys.*, 79:12–49, 1988.
- [21] A. Spira and R. Kimmel. Geodesic curvature flow on parametric surfaces. In *Curve and Surface Design: Saint-Malo 2002*, pages 365–373, Saint-Malo, France, June 2002.
- [22] A. Spira and R. Kimmel. Enhancing images painted on manifolds. In *Proc. of Scale Space 2005, Lecture Notes in Computer Science (vol. 3459)*, pages 492–502, Hofgeismar, Germany, April 2005.
- [23] M. Sussman and E. Fatemi. An efficient interface preserving level set re-distancing algorithm and its application to interfacial incompressible fluid flow. *SIAM J. Sci. Comput.*, 20(4):1165–1191, 1999.